International Journal of Applied Science and Engineering
2014. 12, 4: 241-256

A Numerical Study on Non-Isothermal Flow Through a Rotating Curved Duct with Square Cross Section

Md. Abdul Hye[a] and Md. Mizanur Rahman[b*]

[a] *Departments of Mathematics & Statistics, Bangladesh University of Business & Technology, Dhaka-1216, Bangladesh*
[b] *Department of Mathematics, Faculty of Applied Science and Technology, Islamic University, Kushita-7003, Bangladesh*

Abstract: Non-isothermal flow through a rotating curved duct with square cross section is studied numerically by using the spectral method, and covering a wide range of the Taylor number, Tr, $0 \le Tr \le 2000$ and Dean number, Dn, $0 \le \mathrm{Dn} \le 2000$. A temperature difference is applied across the vertical sidewalls for Grashof number Gr = 500, where the outer wall is heated and the inner one cooled. The rotation (Coriolis force) of the duct about the center of curvature is imposed. The Steady solutions are obtained by using Newton-Raphson iteration method and the Dean numbers are also discussed in detail. Then, in order to investigate the non-linear behavior of the steady and unsteady solutions, there is no stable steady solution, time evolution calculations as well as power spectrum of the periodic oscillations are obtained, and it is also found that for larger Dn, the unsteady flow undergoes in the scenario "steady $\rightarrow$ periodic $\rightarrow$ chaotic $\rightarrow$ steady", if Tr is increased. Finally spectral analysis and phase space are found to be very useful investigation of the Non-isothermal fluid flow behavior.

Keywords: Curved duct; Taylor number; Dean number; secondary flow; curvature; time evolution.

1. Introduction

Due to engineering application and their intricacy, the flow in a rotating curved duct has become one of the most challenging research fields of fluid mechanics. The study of flow through a curved duct is of fundamental interest because of its importance in chemical, mechanical and biological engineering. Since rotating machines were introduce into engineering applications such as gas turbines, electric generators, rooting heat exchangers, cooling system and some separation processes, scientists have paid considerable attention to the characteristics of the flows in these rotating systems. The readers are referred to Berger et al. [1], Nandakumar and Masliyah [2] and Gottlieb et al. [3] for some outstanding reviews on curved duct flows.

Many researchers have performed experimental and numerical investigation on developing and fully developed curved duct flows. Ludwieg [9] first analyzed the flow in a co-rotating (the rotating angular velocity and the axial velocity are in the same direction) curved duct by

* Corresponding author; e-mail: mizan_iu@yahoo.com

Received 12 April 2013
Revised 5 June 2014
Accepted 23 June 2014

integrating the momentum equations. Miyazaki [10] studied the characteristics of the flow and heat transfer in a rotating curved duct rectangular duct with positive rotation. Wang and Cheng [11] studied the characteristics and heat transfer in curved ducts for positive cases and found reverse secondary flow for co-rotation cases. Selmi and Nandakumer [12] and Yamamoto et al. [13] performed extensive works on the rotating curved duct flows and their bifurcations. Yanamoto et al. [13], employing the spectral method, examined the flow structure and the flow rate ratio for the flow in a rotating curved duct and found a six-cell phenomenon in the secondary flow. In their paper, they predicted there should be some multiple solutions but they did not obtain then. Yang and Wang [14] performed comprehensive numerical study on bifurcation structure and stability of solutions for laminar mixed convection in a rotating curved duct of square cross section. The flow through a curved duct with differentially heated vertical sidewalls has other aspects because secondary flows promote fluid mixing and heat transfer in the fluid (Chandratilleke and Nursubyakto [6]). Mondal et al. [7] and Yanse et al. [8] performed numerical investigations of non-isothermal flows through curved ducts with square and rectangular cross sections. While some of such new features are revealed by recent analytical and numerical works (Wang and Cheng [11]; Yang and Wang [14]), there is no known study on bifurcation and stability for forced convection in a rotating curved duct with the study of time–dependent behavior. Recently Mondal et al. [15] performed a comprehensive numerical study of the non-isothermal flows through rotating curved square ducts for small Grashof number ($Gr = 100$). In the present study, we perform numerical study on non-isothermal flow through a rotating curved duct flow for large Grashof number ($Gr = 500$), because we are expected that more completed flow behavior of the unsteady solutions may occur. We setup the range of Taylor number ($0 \le Tr \le 2000$), Dean number ($0 \le Dn \le 2000$) because within the range was carried out the temporal oscillation takes between symmetric/asymmetric two and four-vortex steady solutions. We also showed that the chaotic solution becomes weak for small Dean number, while the chaotic solution becomes strong for large Dean number.

We are developed two-dimensional flow of viscous incompressible fluid and bifurcation structure stability through a rotating curved square duct whose outer wall is heated and inner one is cooled. Flow characteristics are studied over a wide range of the Dean number and the Taylor number by finding the steady solutions, investigating their linear stability and calculating nonlinear behavior of the unsteady solutions by time evolution calculations with phase spaces. Transient behavior of the unsteady solutions, such as periodic, multi-periodic or chaotic solutions are yet unresolved for the non-isothermal flow in a rotating curved duct. This paper is, therefore, an attempt to fill up this gap with the study of stability analysis of multiple solutions.

2. Governing equations

Consider a hydro dynamically and thermally fully developed two-dimensional flow of viscous incompressible fluid through a curved duct with square cross section. Let $2d$ be the width of the cross section. The coordinate system with the relevant notations is shown in Figure 1.

Where C is the centre of the curvature and L is the radius of the curvature. The x and y axes are taken to be in the horizontal and vertical directions respectively, and z is the coordinate along the center-line of the duct, i.e., the axial direction.

It is assumed that the outer wall of the duct is heated while the inner one is cooled. The temperature of the outer wall is $T_0 + \Delta T$ and that of the inner wall is $T_0 - \Delta T$, where $\Delta T > 0$. It is also assumed that the flow is uniform in the axial direction, and that it is driven by a

constant pressure gradient $G\left(G=-\frac{\partial P'}{\partial z'}\right)$ along the center-line of the duct. The main flow in the z direction as in Figure 1.

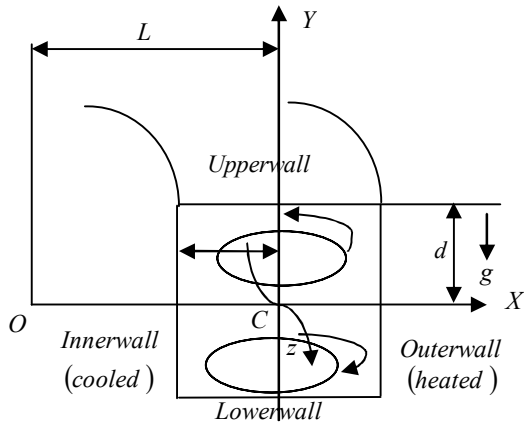

Figure 1. Coordinate system of the curved square duct

The dimensional variables are then non-dimensional zed by using the representative length l, the representative velocity $U_0=\frac{\upsilon}{d}$, where υ is the kinematic viscosity of the fluid. We introduce the non-dimensional variables defined as $u=\frac{u'}{U_0}$, $v=\frac{v'}{U_0}$, $w=\frac{\sqrt{2\delta}}{U_o}w'$, $x=\frac{x'}{d}$, $\bar{y}=\frac{y'}{d}$, $z=\frac{z'}{d}$, $T=\frac{T'}{\Delta T'}$, $t=\frac{U_0}{d}t'$, $\delta=\frac{d}{L}$, $P=\frac{P'}{\rho U_0^{\,2}}$, $G=-\frac{\partial P'}{\partial z'}\frac{d}{\rho U_0^2}$

where u, v and w are the non-dimensional velocity components in the x, y and z directions, respectively; t is the non-dimensional time, P is the non-dimensional pressure, δ is the non-dimensional curvature defined as $\delta=\frac{d}{L}$, and temperature is non-dimensionalized by ΔT. Hence forth, all the variables are non-dimensionalized if not specified.

Since the flow field is uniform in the z direction, the sectional stream function ψ is introduced as:

$$u=\frac{1}{1+\delta x}\frac{\partial\psi}{\partial\bar{y}},\quad v=-\frac{1}{1+\delta x}\frac{\partial\psi}{\partial x} \tag{1}$$

A new coordinate variable y is introduced in the $\bar{y}$ direction as $\bar{y}=a\,y$, where $a=\frac{h}{l}$ is the aspect ratio of the duct cross section. In this study, we consider the case for $h=l$ i.e. $a=1$ (square duct). Then, the basic equations for w, ψ and T are expressed in terms of non-dimensional variables as:

$$(1+\delta x)\frac{\partial w}{\partial t}+\frac{\partial(w,\psi)}{\partial(x,y)}-Dn+\frac{\delta^2 w}{1+\delta x}=(1+\delta x)\Delta_2 w-\frac{\delta}{1+\delta x}\frac{\partial\psi}{\partial y}w+\delta\frac{\partial w}{\partial x} \tag{2}$$

$$\left(\Delta_2 - \frac{\delta}{1+\delta x}\frac{\partial}{\partial x}\right)\frac{\partial \psi}{\partial t} = -\frac{1}{(1+\delta x)}\frac{\partial(\Delta_2\psi,\psi)}{\partial(x,y)} + \frac{\delta}{(1+\delta x)^2}\left[\frac{\partial \psi}{\partial y}\left(2\Delta_2\psi - \frac{3\delta}{1+\delta x}\frac{\partial \psi}{\partial x} + \frac{\partial^2\psi}{\partial x^2}\right) - \frac{\partial \psi}{\partial x}\frac{\partial^2\psi}{\partial x \partial y}\right] + \frac{\delta}{(1+\delta x)^2}\times\left[3\delta\frac{\partial^2\psi}{\partial x^2} - \frac{3\delta^2}{1+\delta x}\frac{\partial \psi}{\partial x}\right] - \frac{2\delta}{1+\delta x}\frac{\partial}{\partial x}\Delta_2\psi + w\frac{\partial w}{\partial y} + \Delta_2{}^2\psi - Gr(1+\delta x)\frac{\partial T}{\partial x} \tag{3}$$

$$\frac{\partial T}{\partial t} + \frac{1}{(1+\delta x)}\frac{\partial(T,\psi)}{\partial(x,y)} = \frac{1}{Pr}\left(\Delta_2 T + \frac{\delta}{1+\delta x}\frac{\partial T}{\partial x}\right) \tag{4}$$

where,

$$\Delta_2 \equiv \frac{\partial^2}{\partial x^2} + \frac{\partial^2}{\partial y^2},\ \frac{\partial(T,\psi)}{\partial(x,y)} \equiv \frac{\partial f}{\partial x}\frac{\partial g}{\partial y} - \frac{\partial f}{\partial y}\frac{\partial g}{\partial x} \tag{5}$$

The non-dimensional parameters Dn, the Dean number, Gr, the Grashof number, and Pr, the prandtl number, which appear in equation (2) - (4) are defined as:

$$Dn = \frac{Gd^3}{\mu\upsilon}\sqrt{\frac{2d}{L}},\ Gr = \frac{\beta g \Delta T\, d^3}{\upsilon^2},\ \mathrm{Pr} = \frac{\upsilon}{\kappa} \tag{6}$$

Where μ, β, κ and g are the viscosity, the coefficient of thermal expansion, the co-efficient of thermal diffusivity and the gravitational acceleration respectively is the viscosity of the fluid. In the present study, only Dn is varied while δ, Gr and Pr are fixed as $\delta = 0.5$, $Gr = 500$ and Pr = 7.0 (water). The rigid boundary conditions used here for w and ψ are as:

$$w(\pm 1, y) = w(x, \pm 1) = \psi(\pm 1, y) = \psi(x, \pm 1) = \frac{\partial \psi}{\partial x}(\pm 1, y) = \frac{\partial \psi}{\partial y}(x, \pm 1) = 0 \tag{7}$$

and the temperature T is assumed to be constant on the walls as:

$$T(1,y) = 1,\ T(-1,y) = -1,\ \ T(x, \pm 1) = x \tag{8}$$

It should be noted that the Equations (2), (3) & (4) are invariant under the transformation of the variables.

$$\left.\begin{aligned} &y \Rightarrow -y \\ &w(x,y,t) \Rightarrow w(x,-y,t), \\ &\psi(x,y,t) \Rightarrow -\psi(x,-y,t), \\ &T(x,y,t) \Rightarrow -T(x,-y,t) \end{aligned}\right\} \tag{9}$$

Therefore, the case of heating the inner sidewall and cooling the outer sidewall can be deduced directly from the results obtained in this study. Equations (2) - (4) would serve as the basic governing equations which will be solved numerically as discussed in the following section.

3. Numerical calculations

The present study is based on numerical calculations to solve the equations (2) - (4), the spectral method is used. This is the method which is thought to be the best numerical method for

solving the Navier-Stokes as well as energy equations (Gottlieb and Orszag, 1997). By this method the variables are expanded in a series of functions consisting of Chebyshev polynomials. The expansion functions $\phi_n(x)$ and $\psi_n(x)$ are expressed as:

$$\left.\begin{aligned}\phi_n(x) &= (1-x^2)C_n(x),\\ \psi_n(x) &= (1-x^2)^2 C_n(x)\end{aligned}\right\} \tag{10}$$

where $C_n(x) = \cos\left(n\cos^{-1}(x)\right)$ is the n^{th} order Chebyshev polynomial. $w(x,y,t), \psi(x,y,t)$ and $T(x,y,t)$ are expanded in terms of the expansion functions $\phi_n(x)$ and $\psi_n(x)$ as:

$$\begin{aligned} w(x,y,t) &= \sum_{m=0}^{M}\sum_{n=0}^{N} w_{mn}(t)\varphi_m(x)\varphi_n(y)\\ \psi(x,y,t) &= \sum_{m=0}^{M}\sum_{n=0}^{N} \psi_{mn}(t)\psi_m(x)\psi_n(y)\\ T(x,,y,t) &= \sum_{m=0}^{M}\sum_{n=0}^{N} T_{mn}\varphi_m(x)\varphi_n(y) + x \end{aligned} \tag{11}$$

where M and N are the truncation numbers in the x and y directions respectively. The collocation points (x_i, y_j) are taken to be

$$\left.\begin{aligned} x_i &= \cos\left[\pi\left(1-\frac{i}{M+2}\right)\right], \qquad i = 1,\ldots,M+1\\ y_j &= \cos\left[\pi\left(1-\frac{j}{N+2}\right)\right], \qquad j = 1,\ldots,N+1\end{aligned}\right\} \tag{12}$$

Wher $i=1, \ldots, M+1$ and $j=1, \ldots, N+1$. Steady solutions are obtained by the Newton-Rapshon iteration method assuming that all the variables are time independent. The convergence is assured by taking sufficiently small ε_p ($\varepsilon_p < 10^{-10}$) defined as:

$$\varepsilon_p = \sum_{m=0}^{M}\sum_{n=0}^{N}\left[\left(w_{mn}^{(p+1)} - w_{mn}^{p}\right)^2 + \left(\psi_{mn}^{(p+1)} - \psi_{mn}^{p}\right)^2 + \left(T_{mn}^{(p+1)} - T_{mn}^{p}\right)^2\right] \tag{13}$$

The present numerical calculation, for sufficiently accuracy of the solutions, we take $M = 20$ and $N = 20$ for a square duct. Finally, in order to calculate the unsteady solutions, the Crank-Nicolson and Adams-Bashforth methods together with the function expansion (11) and the collocation methods are applied to equations (2) - (4).

4. Time-evolution calculation

In order to solve the non-linear time evolution equations, we use the Crank-Nicolson and Adams-Bashforth method. For the Crank-Nicolson method more explicitly, we consider the following one-dimensional heat-flow equation.

$$\frac{\partial q}{\partial t} = \sigma\frac{\partial^2 q}{\partial x^2} \tag{14}$$

where $q(t)$ the temperature is at time t regarded as a function of x and σ is the heat conductivity. The first time derivative in Equation (14) is replaced by a finite difference ratio and

a time step Δt, the derivative with respect to time may be written as:

$$\frac{\partial q}{\partial t} \approx \frac{q(t+\Delta t)-q(t)}{\Delta t} \quad \text{as} \quad \Delta t \to 0$$

Now taking the average at t and $t+1$, Eq. (14) becomes approximately,

$$\frac{q(t+\Delta t)-q(t)}{\Delta t} = \frac{\sigma}{2}\frac{\partial^2}{\partial x^2}[q(t+\Delta t)-q(t)] \tag{15}$$

The approximate solution of equation. (14), thus evaluated, is a function of Δt as well as x and t, and the true solution is the limit of the approximate one as $\Delta t \to 0$. The method, determined by equation. (15), is called the Crank-Nicolson method. The Adams-Bashforth Method, on the other hand, is used for numerically solving initial value problems for ordinary differential equations. This method is an explicit linear multistep method that depends on multistep previous solution points to generate a new approximate solution point.

5. Results and discussion

In this study, we take a curved duct with square cross section and rotate it around the center of curvature with an angular velocity Ω_T. According to the definition of Tr, positive Tr means that the rotational direction is the same as that of the main flow. In the present study, we investigate the flow characteristics only for the case of positive rotation of the duct (positive Tr) and discuss the flow phenomena for the Dean numbers, $Dn = 2000$, over a wide range of the Taylor number $0 \le Tr \le 2000$. Thus, an interesting and complicated flow behavior will be expected if duct rotation is involved for these cases.

5.1. When *Dn = 2000*

5.1.1. Steady solutions

We obtain four branches of steady solutions for $Dn = 2000$ over a wide range of Tr, for $0 \le Tr \le 2000$. The bifurcation diagram of steady solutions is shown in Figure 2. The four steady solution branches are named the first steady solution branch (first branch, thick solid red line), the second steady solution branch (second branch, thick solid blue line), the third steady solution branch (third branch, thick solid green line) and the fourth steady solution branch (fourth branch, thick solid purple line), respectively. The steady solution branches are obtained by the path continuation technique with various initial guesses as discussed in Mondal [7] and are distinguished by the nature and number of secondary flow vortices appearing in the cross section of the duct. In the following, the four steady solution branches along with the flow patterns and temperature profiles on the respective branches are discussed individually.

The first steady solution branch for $Dn = 2000$ is solely depicted in Figure 3(a), for $0 \le Tr \le 2000$. The branch starts from point $a\ (Tr = 0)$ to the direction of increasing Tr as Q decreases which extends up to point d ($Tr = 2000$) without any turning. Then, in order to observe the change of the flow patterns on the first branch, contours of typical secondary flow and temperature profile are drawn at several values of Tr as shown in Figure 3(b), where it is seen that the branch is composed of only two-vortex solutions which are symmetric with respect

to the horizontal plane $y = 0$. Three types of forces, Coriolis force, strong centrifugal force and buoyancy force act on the fluid at the same time, which make the flow patterns symmetric. In the case of temperature profile heat transmission from inner wall to the outer wall by convection becomes more frequent with the increase of rotation (Tr).

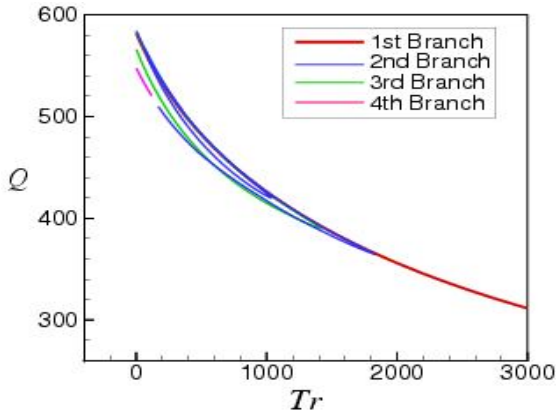

Figure 2. Steady solution branches for $Dn = 2000$

The first steady solution branch:

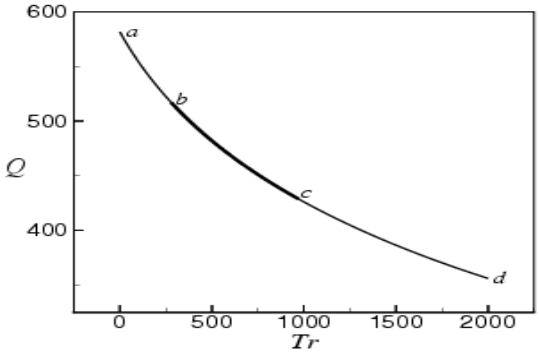

Figure 3(a). First steady solution branch with the region of linear stability (Thick solid line) for $Dn = 2000$.

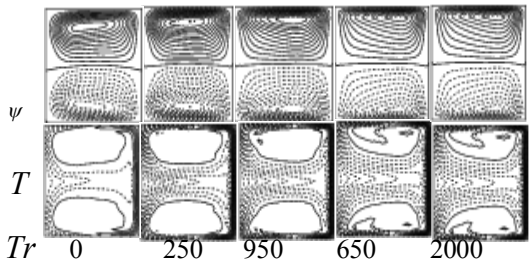

Figure 3(b). Contours of secondary flow (top) and temperature profile (bottom) on the first steady solution branch at several values of Tr.

We draw the second steady solution branch for $Dn = 2000$ separately in Figure 4(a). As seen in Figure 4(a) the branch starts from point a ($Tr = 0$) and goes to the direction of increasing of Tr as Q decreases and drives at point b ($Tr = 1450$) where it turns to the opposite direction

with a gentle turning at point b. The branch then goes to the direction of increasing Q and decreasing Tr up to point c ($Tr = 0$). To observe the change of the flow patterns, contours of typical secondary flow and temperature profile on this branch are shown in Figure 4(b) for several values of Tr. As seen in Figure 4(b), the branch consists of asymmetric two-and nearly symmetric four-vortex solutions. It is found that the secondary flow is a two-vortex solution from point a to point b, but when the branch turns at point b down to point c the secondary flow becomes a four-vortex solution. Linear stability of the steady solution shows that the branch is linearly unstable for any value of Tr.

The Second steady solution branch:

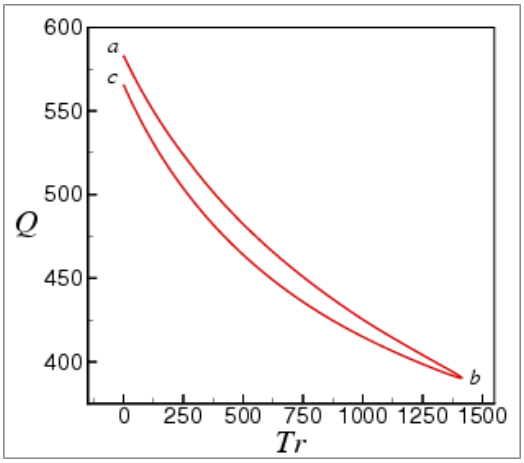

Figure 4(a). Second steady solution branch for $Dn = 2000$.

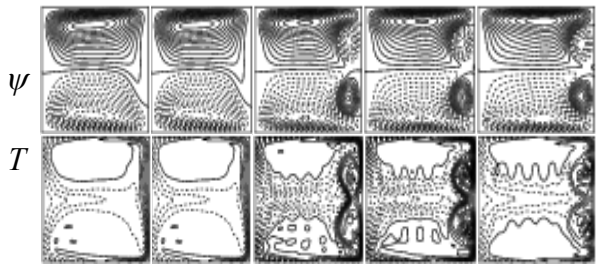

Tr 0 110 450(b-c) 750(b-c) 950(b-c)

Figure 4(b). Contours of secondary flow (top) and temperature profile (bottom) for the second steady solution branch at different values of Tr (from upper branch to the lower)

The third steady solution branch for Dn=2000 shown by a thin solid line in Figure 5(a), the branch is very entangled with many turning points on its way, like the third branch obtained by Yanase et al. [8] for isothermal flow without rotation. We draw the contours of secondary flow and temperature profile at several values of Tr on this branch in Figure 5(b), where it is observed that the branch consists of two- and four- vortex solutions but are different from those of the second steady solution branch. Linear stability of the third steady solution branch shows that the branch is also unstable everywhere.

We draw the fourth steady solution branch for $Dn = 2000$ in Figure 6(a) (thick solid purple line), is solely depicted. Enlargement of this branch is shown in Figure 6(b) in which we found

that the branch has two parts very close to each other, the upper part (a-b) and the lower part (b-c). The branch starts from point *a* and goes to the direction of increasing *Tr* and decreasing *Q* up to point *b* ($Tr = 116.10$), where it experiences a reverse turning andgoes to the direction of increasing *Q* and decreasing *Tr* onwards. To observe the change of the flow patterns and temperature distributions, contours of typical secondary flow and temperature profile on this branch are shown in Figure 6(c), at several values of *Tr*, where it is seen that the branch is composed of asymmetric four-vortex solutions. Linear stability of the fourth branch shows that the branch is also linearly unstable everywhere.

The third steady solution branch:

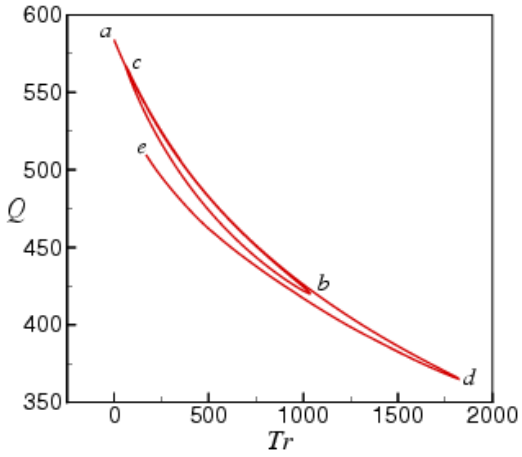

Figure 5(a). Third steady solution branch for $Dn = 2000$.

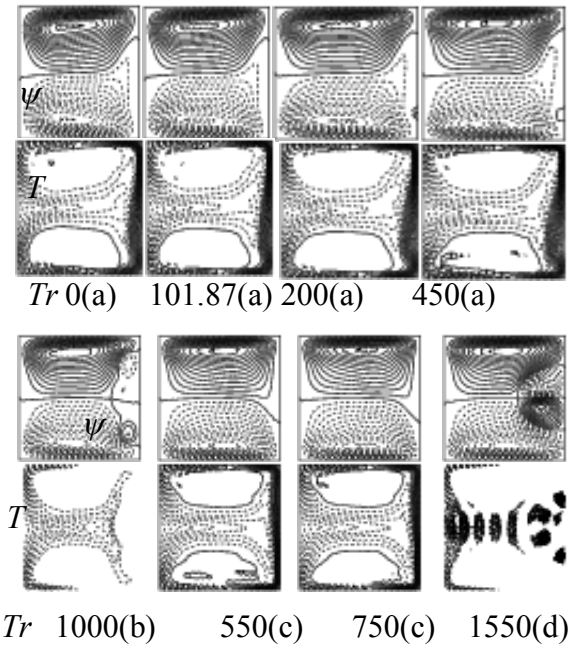

Figure 5(b). Contours of secondary flow (top) and temperature profile (bottom) for the third steady solution branch at different values of *Tr (*from upper branch to the lower).

The Fourth steady solution branch:

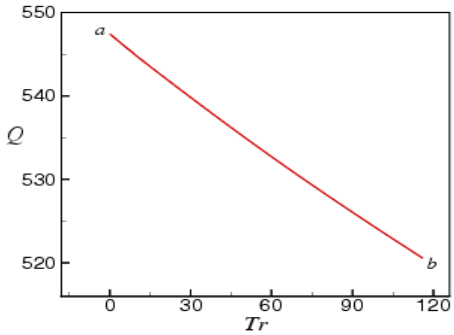

Figure 6(a). Fourth steady solution branch for $Dn = 2000$.

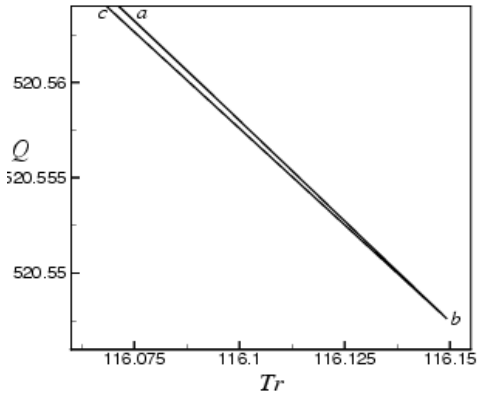

Figure 6(b). Enlargement of fourth steady solution branch for $Dn = 2000$.
branch for $Dn = 2000$.

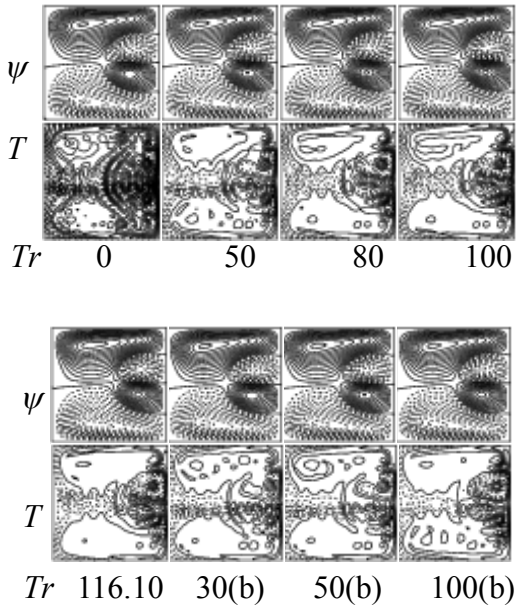

Figure 6(c). Contours of secondary flow (top) and temperature profile (bottom) for the second steady solution branch at different values of *Tr* (from upper branch to the lower).

5.1.2. Linear stability of the steady solutions

Linear stability of first steady solution branch for $Dn = 2000$ shows an interesting result. It is found that the branch is linearly stable in a couple of intervals of *Tr*, one for small *Tr* ($0 \le Tr \le 279$) and another one for larger *Tr* ($922.90 \le Tr \le 2000$). Thus the branch is linearly unstable for the region ($279.1 \le Tr \le 922.80$). The eigenvalues of the first steady solution branch are listed in Table 1, where the eigenvalues with the maximum real part of σ (first eigenvalues) are presented. Those for the linearly stable solutions are printed in bold letters. As seen in Table 1, the perturbation grows oscillatory ($\sigma_i \neq 0$) for $279 \le Tr \le 922.80$ and monotonically ($\sigma_i = 0$) for $Tr \ge 922.80$. Therefore, the *Pitchfork bifurcation* occurs at $Tr = 279.10$ and the *Hopf bifurcation* at $Tr = 922.80$.

Table 1. Linear Stability of the first steady solution branch for $Dn = 2000$ and $Gr = 500$.

Tr	Q	σ_r	σ_i
0	581.665065	-2.0525	0
279.00	517.115175	-2.7722×10^{-4}	8.7596×10
279.10	517.096957	3.2324×10^{-3}	8.7601×10
528.30	478.139438	5.5473×10^{0}	9.5355×10
922.80	433.296084	1.7839×10^{-3}	-9.4593×10
922.90	433.286412	-1.8951×10^{-3}	-9.4591×10
1660.00	375.904510	-3.2206×10^{0}	0
2000.00	356.047431	-3.4120×10^{0}	0

5.1.3. Unsteady solutions

We perform time-evolution calculations of the unsteady solutions for $Dn = 2000$ and $0 \le \mathrm{Tr} \le 2000$. Time evolution of Q for $Dn = 2000$ and $\mathrm{Tr} \le 279$, at which the steady solution is linearly stable on the first branch, shows that the value of Q quickly approaches that of the stable solution on this branch no matter what the initial conditions we use. Then, in order to see what happens when all the steady solutions are linearly unstable in the region $279 \le \mathrm{Tr} \le 922.80$, time evolutions of Q are then performed for $Tr = 400$, 600, 800 and 1000.

Figure 7(a) shows the time-evolutions result for $Tr = 400$ where it is seen that the flow oscillates periodically. In the same figure, to observe the relationship between the periodic solution and the steady states, the values of Q for the steady solution branch at $Tr = 400$ are shown by straight lines using the same kind of lines as were used in the bifurcation diagram in

Figure 7. As seen in Figure 7(a) the solution at $Tr = 400$ oscillates in the region below the upper parts and above the lower parts of the steady solution, there are branches. To observe the periodic change of the flow characteristics and temperature distributions, contours of typical secondary flow and temperature profile for one period of oscillation at $27.25 \le t \le 27.50$ are shown in Figure 7(b), where it is seen that the periodic oscillation at $Tr = 400$ is a two-vortex solution.

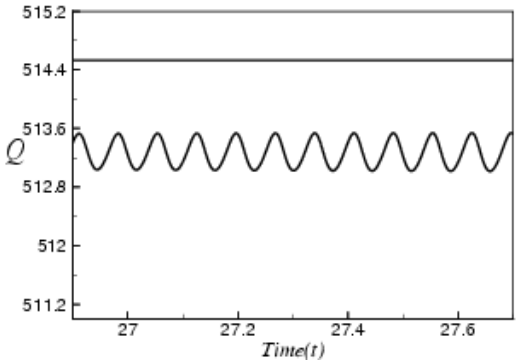

Figure 7(a). Time evolution of Q and the values of Q for the steady solutions for $26.05 \le t \le 27.50$ with unsteady solutions for $Dn = 2000$ and $Tr = 400$.

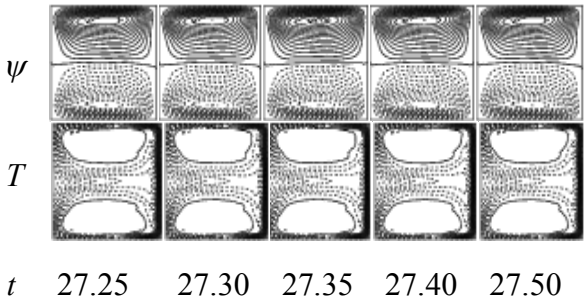

Figure 7(b). Contours of secondary flow (top) and temperature profile (bottom) for one period of oscillation at $27.25 \le t \le 27.50$

Next, the time evolution of Q, for the steady solution branches indicated by straight lines, are shown in Figure 8(a), for Tr = 600. It is found that the flow oscillates periodically in the region along the values of Q on the upper and lower parts of the steady solution branch. The associated secondary flow patterns and temperature profiles at $18.90 \le t \le 19.10$ are shown in Figure 8(b). It is found that the unsteady flow at Tr = 600 also oscillate between the asymmetric two-vortex solutions.

Next, the time evolution of Q together with the values of Q for the steady solution branches, indicated by straight lines, are shown in Figure 9(a) for $Tr = 800$. It is found that the flow oscillates periodically in the region along the values of Q on the upper parts of the steady solution branch. The associated secondary flow patterns and temperature profiles at $10.50 \le t \le 10.70$ are shown in Figure 9(b). It is found that the unsteady flow at $Tr = 800$ also oscillates between the asymmetric two-vortex solutions.

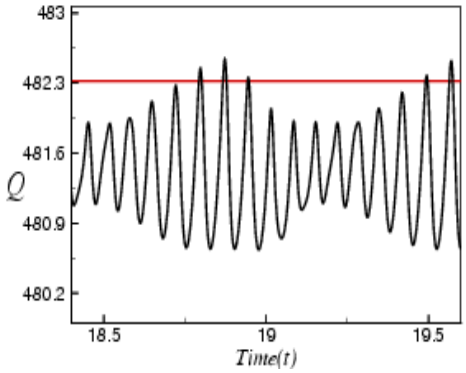

Figure 8(a). Time evolution of Q and the values of Q for the steady solutions for $18.0 \le t \le 19.7$ with unsteady solutions for $Dn = 2000$ and $Tr = 600$.

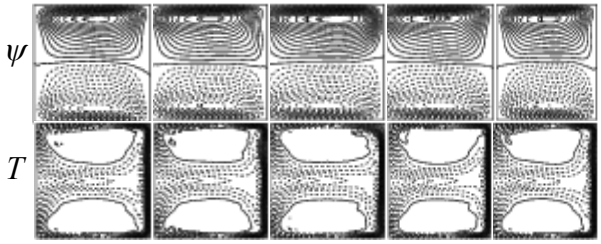

t 18.90 18.95 19.00 19.05 19.10

Figure 8(b). Contours of secondary flow (top) and temperature profile (bottom) for one period of oscillation at $18.90 \le t \le 19.10$.

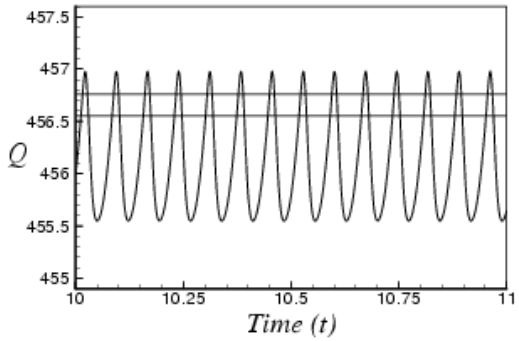

Figure 9(a). Time evolution of Q and the values of Q for the steady solutions for $10 \le t \le 11$ with unsteady solutions for $Dn = 2000$ and $Tr = 800$.

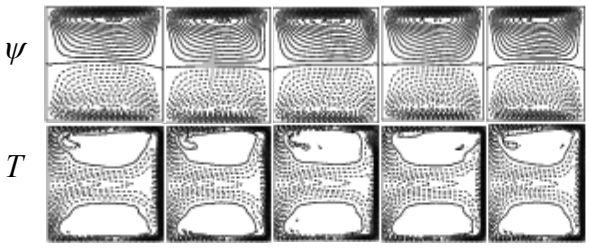

t 10.50 10.55 10.60 10.65 10.70

Figure 9(b). Contours of secondary flow (top) and temperature profile (bottom) for one period of oscillation at $10.50 \le t \le 10.70$.

Similarly, the time evolution of Q together with the values of Q for the steady solution branches, indicated by straight lines, are shown in Figure 10(a) for $Tr = 1000$. It is found that the flow oscillates periodically in the region along the values of Q on the lower part of the steady solution branch. The associated secondary flow patterns and temperature profiles for one period at $7.80 \le t \le 8.00$ are shown in Figure 10(b). It is found that the unsteady flow at $Tr = 1000$ also oscillate between the asymmetric two-vortex solutions. Time evolutions of Q are then performed at several values Tr for $922.90 \le Tr \le 2000$, and it is found that the value of Q approaches steady state. The reason is that the steady flow is stable on the first steady solution branch in this region.

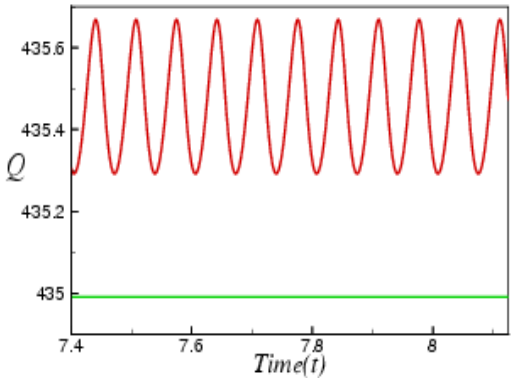

Figure 10(a). Time evolution of Q and the values of Q for the steady solutions for $7.4 \le t \le 8.20$ with unsteady solutions for $Dn = 2000$ and $Tr = 1000$.

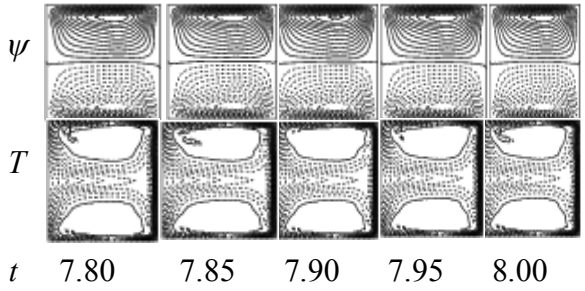

Figure 10(b). Contours of secondary flow (top) and temperature profile (bottom) for one period of oscillation at $7.80 \le t \le 8.00$.

6. Conclusions

In this study, a detailed numerical study on fully develop two-dimensional flow of viscous incompressible fluid through a rotating curved duct with square cross section has been analyzed by using the spectral method over a wide range of the Taylor number, $0 \le Tr \le 2000$ and the Dean number, $0 \le Dn \le 2000$ for the curvature $\delta = 0.1$ Though the present study covers a wide range of Dn, $Dn = 2000$ have been discussed in detail with a temperature difference between the vertical sidewalls for the Grashof number $Gr = 500$, where the outer wall is heated and the inner one cooled.

After a comprehensive survey over the parametric ranges, a single branch of asymmetric

steady solution is obtained for $Dn = 2000$ on the other hand, we obtain four branches of symmetric/asymmetric steady solutions, respectively. It is found that there exist two-and four-vortex solutions on various branches. These vortices are generated due to the centrifugal force and Coriolis force or by their combinations. It is found that as *Dn* increases the number of steady solutions also increases. Linear stability of the steady solutions reveals an interesting result. Time evolution calculations as well as their spectral analyses show that in the unstable region for $Dn = 2000$ the unsteady flow becomes periodic before turning to steady state. In the unstable region for $Dn = 2000$ on the other hand, the unsteady flow becomes periodic first, then multi-periodic, then chaotic and finally turns into steady state again, if *Tr* is increased. In order to investigate the transition from multi-periodic oscillations to chaotic states more explicitly, the orbit of the solution is drawn in phase space.

References

[1] Berger, S. A., Talbot, L., and Yao, L. S. 1983. Flow in Curved Pipes. *Annu. Rev. Fluid. Mech.*, 35: 461-512.

[2] Nandakumar, K. and Masliyah, J. H. 1986. Swirling Flow and Heat Transfer in Coiled and Twisted Pipes. *Adv. Transport Process*, 4: 49-112.

[3] Gottlieb, D. and Orazag, S. A. 1977. "*Numerical Analysis of Spectral Methods"*. Society for Industrial and Applied Mathematics. Philadelphia.

[4] Winters, K. H. 1987. A Bifurcation Study of Laminar Flow in a Curved Tube of Rectangular Cross-section. *J. Fluid Mech*, 180: 343-369.

[5] Mess, P. A. J., Nandakumar, K., and Masliyah J. H. 1996. Steady Spatial Oscillations in a Curved Duct of Square Cross-section. *Phy. Fluids*, 8, 12: 3264-3270.

[6] Chandratilleke, T. T. and Nursubyakto. 2003. Numerical Prediction of Secondary Flow and Convective Heat Transfer in Externally Heated Curved Rectangular Ducts. *Int. J. Thermal Sci.*, 42: 187-198.

[7] Mondal, R. N., Kaga, Y., Hyakutake, T., and Yanase, S. 2006a. Effects of curvature and Convectiv heat Transfer in Curved Square Duct Flows. Trans. ASME, *Journal of Fluids Engineering*, 128, 9: 1013-1022.

[8] Yanse, S., Mondal, R. N., and Kaga, Y. 2005. Numerical Study of Non-isothermal Flow with Convective Heat Transfer in a Curved Rectangular Duct. *Int. J. Thermal Sci.*, 44: 1047-1060.

[9] Ludwieg, H. 1951. Die Ausgebildete Kanalatromung in Einem Rotierenden System. *Ingenieu-archiv*, 19: 296-308.

[10] Miyazaki, H. 1973. Combined Free and Force Convection Heat Transfer and Fluid Flow In Rotating Curved Rectangular Tubes. *Trans. ASME C: J. Heat Transfer*, 95: 64-71.

[11] Wang, L. Q. and Cheng, K. C. 1996. Flow Transitions and combined Free and Forced Convective Heat Transfer in Rotating Curved Channels: the Case of Positive Rotation. *Phys. Of Fluids*, 8: 1553-1573.

[12] Selmi, M. and Namdakumar, K. 1999. Bifurcation Study of the Flow Through Rotating Curved Ducts. *Phys. Of Fluids*, 11: 2030-2043.

[13] Yamamoto, K., Yanse, S., and Alam, M. M. 1999. Flow Through a Rotating Curved Duct with Square Cross-section. *J. Phys. Soc. Japan*, 68: 1173-1184.

[14] Yang, T. and Wang, L. 2003. Bifurcation and Stability of Forced Convection in Rotating Curved Ducts of Square Cross Section. *Int. J. Heat Mass Transfer*, 46: 613-629.

[15] Mondal, R. N., Alam M. M., and Yanase, S. 2007. Numerical Prediction of non-isothermal

flows through a rotating Curved duct with square cross section. *Thommasat Int. J. Sci and Tech.*, 12, 3: 24-43.